JPE 18-1-15

https://doi.org/10.6113/JPE.2018.18.1.160
ISSN(Print): 1598-2092 / ISSN(Online): 2093-4718

An Improved Multi-Tuned Filter for High Power Photovoltaic Grid-Connected Converters Based on Digital Control

Guangyu Sun†, Yongli Li*, and Wei Jin*

†,*Department of Electrical Engineering and Automation, Tianjin University, Tianjin, China

Abstract

For high power photovoltaic (PV) grid-connected converters, high order filters such as multi-tuned filters and *Traps+RC* filters with outstanding filtering performance have been widely researched. In this paper, the optimization of a multi-tuned filter with a low damping resistance and research on its corresponding control scheme have been combined to improve the performance of the proposed filter. Based on the characteristics of the switching harmonics produced by PWM, the proposed filter is optimized to further improve its filtering performance. When compared with the more common *Traps+RC* filter, the advantages of the proposed filter with low damping resistances in attenuating the major switching harmonics have been demonstrated. In addition, a simpler topology and reduced power loss can be achieved. On the other hand, to make the implementation of the proposed filter possible, on the base of the unique frequency response characteristic of the proposed filter, a digital single-loop control scheme has been proposed. This scheme is a simple and effective means to suppress the resonance peak caused by a lack of damping. Therefore, a smaller volume, better efficiency of the proposed filter, and easy implementation of the corresponding control scheme can be realized. Finally, the superiority of the proposed filter topology and control scheme is verified in experiments.

Key words: Digital control, High power grid-connected photovoltaic converter, PWM, Resonance peak

I. Introduction

Recently, high power grid connected photovoltaic (PV) three-phase Voltage-Source Converters (VSCs) have attracted a lot of attention since they are essential for PV power plants [1]. Large amounts of high frequency switching harmonics are produced in the PWM process, which is widely adopted for PV three-phase converters. Because of their good high frequency attenuation performance, *LCL* filters and other filters with branches have been widely applied as the passive filter between VSCs and the utility grid [2], [3]. However, when compared with regular DC/AC converters, there are stricter restrictions on the output filters of high power photovoltaic grid-connected converters due to their operating features. The major restrictions are outlined as follows. 1) Since the structure of high power photovoltaic grid-connected converters is mainly single-staged for better efficiency, the DC link voltage varies under the influence of MPPT, which changes the distribution of the high frequency switching harmonics. To comply with the distortion limits on current harmonics specified by IEEE regulations in different cases, better attenuation performance for the switching harmonics of the filters is required. 2) High power PV grid-connected converters usually operate at a relatively low switching frequency (2kHz-4kHz), which leads to the low frequency harmonic currents being injected into the grid. In such cases, the output filters, which are based mainly on inductance, could not perform well in attenuating these harmonics [4]. 3) The stability of a grid-connected converter system is difficult to achieve with an active damping method, due to the relatively long digital delay caused by a low switching frequency [22]. When a passive damping method is applied, relatively high damping resistances in branches are required to guarantee system stability, which increases the total power loss of the system. Restrained by the above restrictions, for a high power PV grid-connected converter, large inductance and volume are required for the output filter to ensure

Manuscript received Dec. 2, 2016; accepted Sep. 12, 2017
Recommended for publication by Associate Editor Se-Kyo Chung.
†Corresponding Author: 1262543289@qq.com
Tel: +86-13920175090, Tianjin University
*Dept. of Electrical Eng. and Automation, Tianjin University, China

sufficient filtering performance [4]. In addition, the efficiency of the PV system is obviously decreased. The cost of the filter inductance is around 20% up to 30%, while the volume of the passive components is from 30% up to 50% of the whole converter system [5]. Therefore, a filter topology which can achieve better filtering performance with a smaller inductance and volume is necessary for high power PV three-phase grid-connected converters.

A multi-tuned filter, with 2 or 3 paralleled *LC* traps instead of the capacitor branch of a *LCL* filter, has already been proposed based on a *LCL* filter [6]. Since the switching harmonics mainly centralize around the switching frequency (f_s) and its multiples (nf_s) [7], by introducing the *LC* trap branches, much better harmonic attenuations can be achieved for multi-tuned filters on these harmonics when compared with a *LCL* filter. Thus, the inductance and volume of the passive filter can be further reduced. However, for multi-tuned filters, the damping resistor in each of the *LC* trap branches severely weaken the harmonic attenuation capability around f_s and nf_s. Thus, a filter topology derived from a multi-tuned filter, named 2*Traps*+*RC* filter, was proposed in [8]. By inserting an additional *RC* branch in parallel with the *LC* branches and removing the damping resistors of the *LC* branches, the resonance of the 2*Traps*+*RC* filter is properly damped by the resistor of the *RC* branch. In addition, good harmonic attenuation performance around f_s and $2f_s$ can be guaranteed. Similar *Traps*+*RC* filter topologies have been proposed and compared in [9], and optimization methods for these filters to achieve better harmonic attenuation performance and reduced power loss were studied in [10]. However, although the design of the filter topology is closely related to the study of the control scheme, there are few researches on the control schemes for these high order filters. Common control schemes for these filters are mainly based on a *PI* or *PR* controller in the s-domain [11], [12]. However, for these control schemes, deviations between the real model and the established control model are obvious when applied in high power PV converters with a low control frequency. In addition, the stability of the control schemes is highly dependent on the damping resistance of the filter.

In this paper, an improved multi-tuned filter topology for high power grid-connected PV converters based on the control scheme design is proposed. Based on the characteristics of the switching harmonics produced by PWM, the parameters of a multi-tuned filter with a low damping resistance, especially the stages of the proposed filter and the damping resistors in the *LC* traps, are optimized. The improved filter is characterized by its enhanced general harmonic attenuation performance for switching harmonics, simpler topology and reduced power loss, when compared with the more common *Trap*+*RC* type filter. On the other hand, considering the frequency response characteristic of the proposed topology, the impact of the resonance peak on system stability is settled with a digital control scheme. In terms of the digital single-loop control scheme for a *LCL* filter [13], [14], a single-loop controller based on grid side current feedback for a multi-tuned filter, which effectively suppresses the resonance peak, is designed.

To highlight the superiority of the improved multi-tuned filter and the corresponding single-loop control scheme, the rest of this paper is organized as follows. Section II explains the improvements to the multi-tuned filter topology in detail, and analyzes the filtering performance of the proposed filter by means of a comparison. In section III, a single-loop controller with grid current feedback for the proposed filter is concretely designed. In Section IV, comparative experiments are carried out to validate the excellent harmonic attenuation of the proposed filter and the feasibility of the proposed control scheme.

II. IMPROVEMENTS OF THE MULTI-TUNED FILTER

The proposed filter topology in a PV VSC system is shown in Fig. 1, which consists of a grid coupling inductor, L_g, a ripple inductor, L_i, and *RLC* shunt traps between them. This is similar to the conventional multi-tuned filter in [6]. To enhance the filtering performance of the multi-tuned filter 0+ and facilitate the implementation of the corresponding control scheme, the improvements in this paper mainly focus on the three aspects. 1) Selection of the series resistor in the *LC* traps. 2) Optimal number of *LC* traps. 3) Selection of the location of the resonance peak. The design principles for the high order filters in [15], [16] can be used for the rest of the design of the improved multi-tuned filter.

A. Selection of the Series Resistor in LC Traps

For the conventional multi-tuned filter, a large damping resistor restrains the harmonic current absorption quantity of the *LC* traps. Thus, the quality factor *Q* of the *LC* traps is limited to be lower than 2. Meanwhile for the low voltage applications of *LC* traps without extra damping, the *Q* factor is usually set between 10 and 60 [17]. However, a higher *Q* in *LC* traps, especially when several *LC* traps are paralleled, may cause potential resonance due to grid-side events such as faults or tap change situations. Therefore, the *Q* factor is chosen around 10-20 for security purposes. This is done at the cost of the certain decrease in terms of harmonic attenuations.

By setting the *Q* factor around 10-20, there are much better harmonic attenuations around the switching frequency (f_s) and its multiples when compared with the conventional multi-tuned filter, which is shown in Fig. 2. In addition, thanks to the reduction of the damping resistors in the branches, improvement in the efficiency of the PV VSC system can also be expected.

B. Optimal Number of LC Traps

The number of *LC* traps is set at 2 or 3 for the conventional

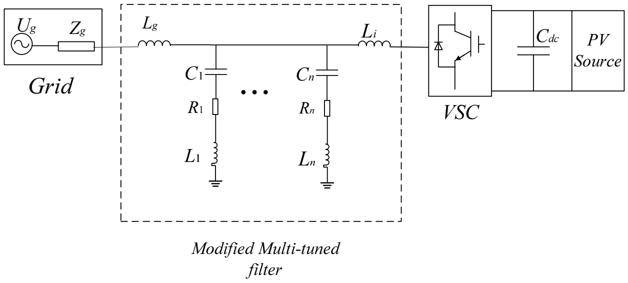

Fig. 1. PV VSC system with a single-phase equivalent circuit of the improved multi-tuned filter topology.

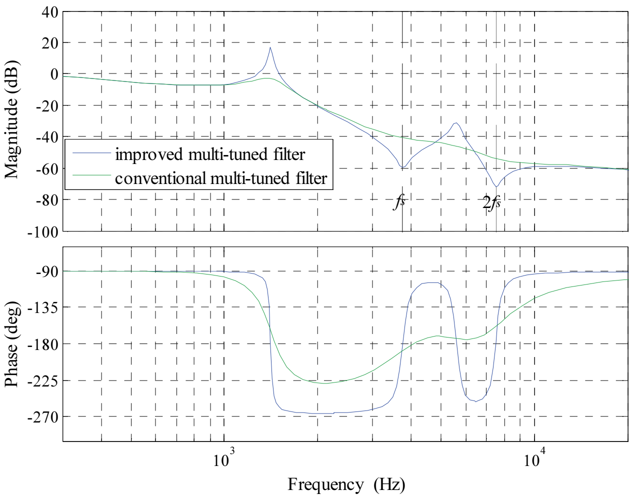

Fig. 2. Bode diagrams of the transfer function $Ig(s)/Ui(s)$ of the conventional and improved multi-tuned filters.

multi-tuned filter in [6]. To further optimize the number of *LC* traps, AM-F curves of the compared multi-tuned filters (2 *LC* traps and 3 *LC* traps) with limits on the harmonic attenuations are analyzed in Fig. 3(a). It is shown in Fig. 3(a) that the harmonic attenuations required to meet IEEE regulations are mainly centralized around nf_s (n=1,2,3…). The *LC* traps aimed for harmonics at around nf_s (n=1,2,3…) largely strengthen the attenuation performance around these frequencies and maximize the advantage of tuned-type high order filters.

To intuitively compare the harmonic attenuation capabilities and to optimize the number of *LC* branches, the magnitude margins for the dominated harmonics of both filters to satisfy IEEE regulations by theoretical calculations are shown in Fig. 3(b). With the help of a grid coupling inductor L_g and a ripple inductor L_i, large enough magnitude margins can be guaranteed at around $3f_s$ and higher frequency bands for multi-tuned filters with 2 *LC* traps. Multi-tuned filters with 2 *LC* traps provide better harmonic attenuations at around f_s and $2f_s$, where most harmonic attenuations are required. In addition, they also guarantee large enough magnitude margins for other harmonic bands. By referring to the "cask principle" in evaluating general filtering performance, multi-tuned filters with 2 *LC* traps provide

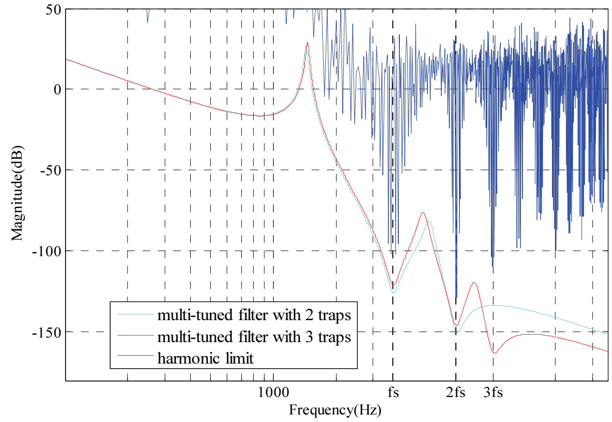

(a)

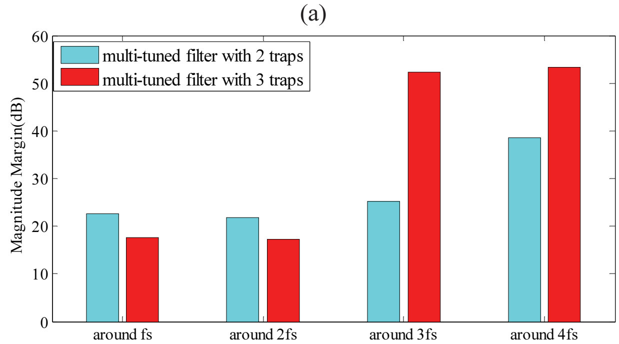

(b)

Fig. 3. Filtering performance comparison when the number of *LC* traps is 2 and 3: (a) AM-F curves of the compared multi-tuned filters with limits on the harmonic attenuations; (b) theoretical magnitude margins for the dominated harmonics of both filters.

more balanced harmonic attenuations at around the dominant harmonic bands, which is a better choice. On the other hand, broader attenuation bands at around f_s and $2f_s$ can be guaranteed in case of a parameter drift as shown in Fig. 3(a). The reduction of a *LC* trap also simplifies the topology structure of the proposed multi-tuned filter. Thus, the optimal number of *LC* traps is fixed to 2 in this paper.

C. Selection of the Location of the Resonance Peak

There are two resonance peaks for the proposed filter as shown in Fig. 2: f_{res1} lower than f_s, and f_{res2} between f_s and $2f_s$. The locations of the resonance peaks affects the filtering performance of the proposed filter and the digital control strategy. f_{res1} is assumed to be placed in a range between $10f_0$ and $0.5f_s$ to avoid oscillations and harmonic amplifications. Thanks to the outstanding attenuation characteristic of the proposed filter at around f_s and f_{res1} could be set more close to $0.5f_s$. In this paper, f_{res1} is set between $1/3f_s$ and $1/2f_s$ to guarantee the application of the proposed control scheme, and f_{res2} is placed at around $1.5f_s$ to limit the harmonics around f_s and $2f_s$. Estimations of the resonance frequencies of the proposed filter with their limitations can be shown in (1) and (2):

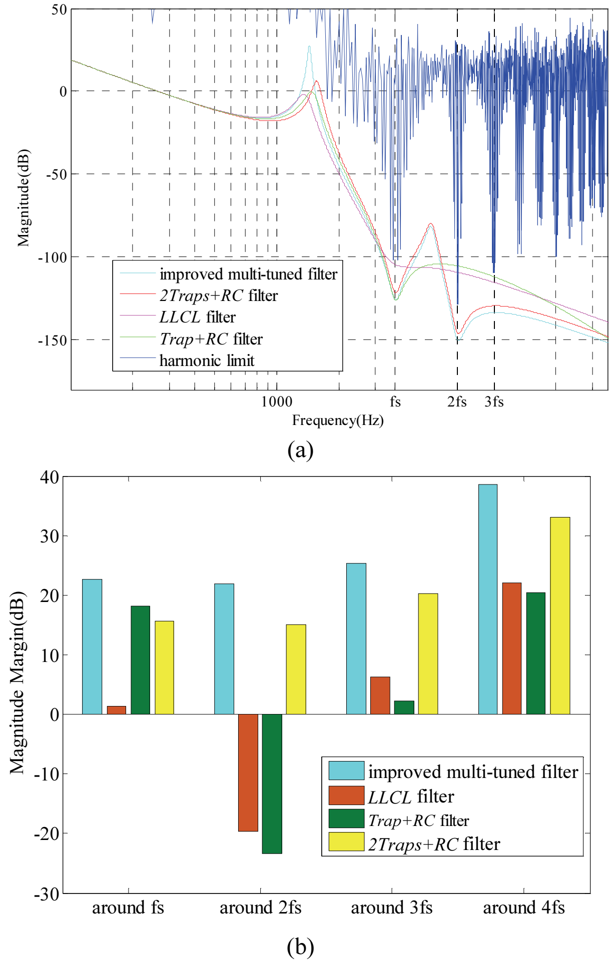

Fig. 4. Filtering performance comparisons of the proposed filter and other common high order filters: (a) AM-F curves of the compared filters with limits on the harmonic attenuations; (b) theoretical magnitude margins for the dominant harmonics of the compared filters.

$$\frac{1}{3}f_s < f_{res1} \approx \frac{1}{2\pi}\sqrt{\frac{L_i + L_g}{L_i L_g (C_1 + C_2)}} < \frac{1}{2}f_s \tag{1}$$

$$f_{res2} \approx \frac{1}{2\pi}\sqrt{\frac{C_1 + C_2}{(L_1 + L_2)C_1 C_2}} \approx 1.5 f_s \tag{2}$$

The similar algorithm in (1) can be used here to optimize the relationship between the parameters of the inductor and capacitor of the proposed filter. The derived overall transfer function $G_{U_i \to I_g}(s)$ of the improved multi-tuned filter is presented in equation (3) (the derivation can be seen in Appendix A).

$$G_{U_i \to I_g}(s) = \frac{as^4 + bs^3 + cs^2 + ds + e}{fs^5 + gs^4 + hs^3 + is^2 + js} \tag{3}$$

where $a=C_1C_2L_1L_2$,
$b= C_1C_2L_1R_2+C_1C_2L_2R_1$,
$c=C_1L_1+C_2L_2+C_1C_2R_1R_2$,
$d=C_1R_1+C_2R_2$,
$e=1$,
$f=C_1C_2L_1L_2(L_g+L_i)+C_1C_2L_gL_i(L_1+L_2)$,
$g=C_1C_2R_2(L_1L_g+L_1L_i+L_gL_i)+C_1C_2R_1(L_2L_g+L_2L_i+L_gL_i)$,
$h=C_1L_1(L_g+L_i)+C_2L_2(L_g+L_i)+L_gL_i(C_1+C_2)+C_1C_2R_1R_2(L_g+L_i)$,
$i=C_1L_gR_1+C_2L_gR_2+C_1L_iR_1+C_2L_iR_2$,
$j= L_g+L_i$

D. Filtering Performance Comparison

In [8]–[11], three other high order tuned-type filters with good filtering performance (*LLCL* filter, *Trap+RC* filter and 2*Traps+RC* filter) were also proposed for grid-connected converters. To highlight the filtering performance of the proposed filter, AM-F curves of the proposed filter and the three tuned-type filters mentioned above are compared with limits on the harmonic attenuations in Fig. 4(a). The totals of the peak storage energy of the passive components in the four compared filters are similar to guarantee the equality of the comparison. The magnitude margins of the dominant harmonics of the compared filters by theoretical calculation are also shown in Fig. 4(b). It can be derived from the broader magnitude margins of the proposed filter in Fig. 4 (b) that the improved multi-tuned filter can reach better and more balanced harmonic attenuations at the dominant harmonic bands than the other common high order filter topologies. This demonstrates the superior generalized filtering performance of the improved multi-tuned filter. When applied to high power PV converters, the superior performance in terms of attenuating the dominant harmonic bands can effectively meet the distortion limits specified by IEEE1547 with reduced total inductance and volume. On the other hand, the reduction of the resistance in the *LC* branches can raise the efficiency of high power PV systems. Thus, the economy of high power PV systems is improved by the improved multi-tuned filter.

III. Digital Control Scheme of a Grid-Connected Converter With the Proposed Filter

Although great filtering performance can be achieved by the proposed filter, oscillations happen due to the lack of damping around f_{res1} for the improved multi-tuned filter. However, since f_{res2} is placed higher than the digital control frequency for different PWM modes, it cannot influence the digital control system. On the other hand, the resonance peak at f_{res2} can be sufficiently damped by the series resistor in the *LC* branch as shown in Fig.3. Therefore, the resonance peak at f_{res2} does not cause oscillations in the control system.

For the proposed filter, the widely adopted passive damping and active damping for the *LCL* filter are unsuitable. The added damping resistors in passive damping greatly weaken the harmonic attenuation at around f_s or $2f_s$ and inevitably decrease the efficiency of the overall system [18]. On the other hand, the multi-loop active damping methods

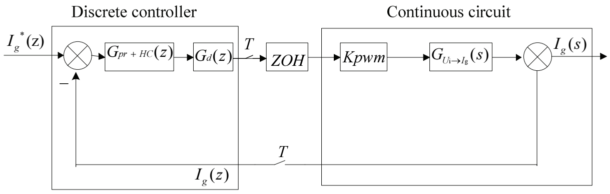

Fig. 5. Block diagram of a single-loop controller with grid-side current feedback in the z-domain.

introducing extra feedback [19]–[21] are also less effective in high power PV converters. Because of the relatively long digital delay caused by the low switching frequency, system stability becomes difficult to achieve [22]. In this paper, by establishing a digital control scheme based on the frequency response characteristic of the proposed topology, a single-loop controller with grid-side current feedback without damping resistances is adopted to deal with oscillations. In [23], it is shown that the essence of the control system stability for the *LCL* filter is strongly related to the location of the resonance frequency and the total equivalent delay time as shown in (4).

$$-2\pi < -\frac{1}{2}\pi - f_{res1} \times T_{delay} \times 2\pi < -\pi \tag{4}$$

where T_{delay} is the total equivalent delay time of the digital control process. The principle is still suitable for the proposed filter, since only one resonance peak exists in the digital control frequency band for both the *LCL* filter and the proposed filter. T_{delay} consists of two parts: the delay time from sampling the PWM output, and the equivalent delay time of the digital PWM process which is equivalent to a sample-and-hold unit [24]. In general, assuming that T_s is a switching period of the converter, for the asymmetric regular sampling PWM methods and the symmetric regular sampling PWM methods (the most commonly applied in the PWM converters [25]), T_{delay} varies from $3T_s/4$ to $3T_s/2$. Then, it can be derived from (4) that a relatively high resonance frequency f_{res1} is required for the implementation of the proposed control scheme.

The greatly reduced total inductance of the improved multi-tuned filter enables a much higher f_{res1}, which is set between $1/3f_s$ and $1/2f_s$ as mentioned in Section II. Thus, the proposed filter is suitable for the adoption of a single-loop controller with grid-side current feedback. For the proposed filter, the restrictions on the single-loop control applications are satisfied under different PWM modes and the output switching harmonics can be effectively limited.

A. Modeling of the Single-Loop Controlled System in the z-domain

In this section, a single-loop controller with grid-side current feedback is modeled in the z-domain to study the stability of the system. The z-domain model accurately indicates the inherent delay nature of the digital control implementation, which is essential for predicting the stability boundaries and designing the proposed controller.

A block diagram of a single-loop controller with grid side current feedback in the discrete domain is depicted in Fig. 5 [26], where $G_{Ui \to Ig}(s)$ is the transfer function stated in (3). In the control system modeling, the inserted low resistances have been neglected. This is done to represent the worst case un-damped scenario. $G_d(z)$ and *ZOH* represent the delay from the sampling to the PWM output, and the equivalent sample-and-hold unit of the digital PWM process, and $G_{pr+HC}(z)$ is a quasi-resonant *PR*+*HC* regulator in the z-domain.

To achieve the accurate tracking of the reference current and mitigation of the selected 5th and 7th harmonics, a quasi-resonant *PR*+*HC* controller is applied under *αβ* static coordinates. The expressions in the s-domain can be seen as follows.

$$Gpr(s) = Kp + Kr\frac{2\xi\omega_0 s}{s^2 + 2\xi\omega_0 s + \omega_0^2} \tag{5}$$

$$GHC(s) = \sum_{h=5,7} Krh\frac{2\xi_h h\omega_0 s}{s^2 + 2\xi_h h\omega_0 s + \omega_0^2} \tag{6}$$

By using abi-linear transformation, $G_{pr}(z)$ is derived in equation (15) as the discrete equivalent of $G_{pr}(s)$. $G_{HC}(z)$ can be transformed into the *z*-domain in the same way.

$$Gpr(z) = Kp + Kr\frac{az^2 + bz + c}{Az^2 + Bz + C} \tag{7}$$

where $A = 4/Ts^2 + 4\xi\omega_0/Ts + \omega_0^2$, $B = -8/Ts^2 + 2\omega_0^2$, $C = 4/Ts^2 - 4\xi\omega_0/Ts + \omega_0^2$, $a=4\xi\omega/T_s$, $b=0$ and $c=-4\xi\omega/T_s$.

The continuous circuit $G_{Ui \to Ig}(s)$ can be transformed into a discrete domain function $G_{Ui \to Ig}(s)$ by applying the ZOH transform with a sampling period of $T=T_{sam;le}$ [25] ($T_{sam;le}=0.5T_s$ for the asymmetric regular sampling PWM, and $T_{sam;le}=T_s$ for the symmetric regular sampling PWM).

Finally, these transfer functions can be combined to create the transfer function of the open-loop forward path expression $G(z)$ for the regulators in Fig. 5. Then, control system analysis techniques such as frequency response (Bode diagram) and pole-zero maps can be applied. For the single-loop control system, the forward path transfer function $G(z)$ is established as:

$$G(z) = KpwmGd(z)G_{pr+HC}(z)G_{Ig \to Ui}(z) \tag{8}$$

B. Stability Analysis of the Proposed System and Selection of the Delay Time

To analyze the stability of the single-loop system, bode diagrams of the open-loop system with three typical T_{delay} ($3T_s/4$, T_s and $3T_s/2$), which are based on the z-domain transfer function discussed above, are shown in Fig. 6. The AM-F characteristics are almost the same for different delay times. The major difference created by the different delay

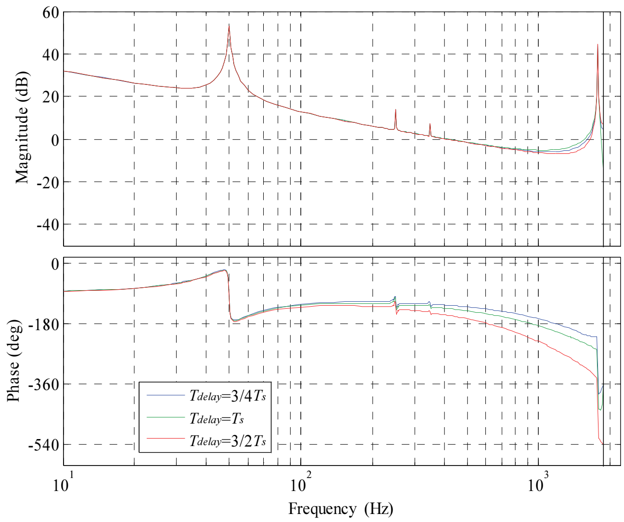

Fig. 6. Bode diagrams of the proposed open-loop system with three typical different T_{delay}.

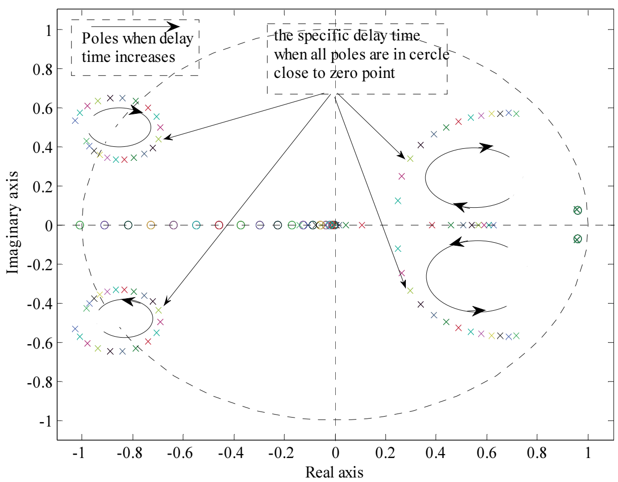

Fig. 7. Pole-zero map of a closed-single-loop system when T_{delay} varies from 0 to $2T_s$.

times is the phase deviation of the PH-F curve. It is depicted in Fig.6 that the phase roll-off created by the delay time causes the PH-F curve to transit below -180° before a relatively high resonance frequency. Thus, large magnitude excursions across 0dB at f_{res1} do not have an influence on system stability. In this way, the whole control system is stabilized.

To determine the desired delay time for system stability, pole-zero maps when T_{delay} varies from 0 to $2T_s$ are illustrated in Fig. 7. The pole-zero maps intuitively show the variation tendency of the system stability when the delay time varies. As T_{delay} grows, two poles gradually move into the circle and then move out of the circle. The specific delay time where all of the poles are in the circle and close to the zero point is selected as T_{delay}, and the corresponding PWM mode is adopted. In this case, large enough stability margins can be guaranteed.

C. Parameter Determination of the Controller

After T_{delay} is settled, the parameter design of the *PR+HC* regulator is proposed in this section. It is clear from Fig.6 that the cutoff frequency should be located lower than the phase crossover point, which is far from f_{res1}. This can be recognized as the same mechanism that limits the performance of simple *L* filter systems [27]. Hence, when designing the controller gains for the proposed system, methods similar to those used for standard *L* filters could be considered, where $L = L_i + L_g$.

First, to design the *PR+HC* regulator, the proportional gain K_p is set to achieve a unity gain at the desired cutoff frequency [28]:

$$Kp \approx \frac{fc(Li + Lg)}{Kpwm} \tag{9}$$

where f_c represents the cutoff frequency, which is highly dependent on the desired phase margin φ_m:

$$fc = \frac{1}{360}\frac{90 - \varphi_m}{Ts} \tag{10}$$

The designing of K_r should ensure that the magnitude of the controller at f_0 is large enough, which can guarantee low steady-state amplitude errors at the fundamental frequency. The current errors ΔI can be derived as (11), which should be less than 5% of the rated RMS current.

$$\Delta I = \frac{Ug}{Kpwm(Kp + Kr)} \le 5\% In \tag{11}$$

where U_g is the rated RMS phase voltage of the grid, and I_n is the rated RMS current.

On the other hand, K_r and K_{rh} (h=5, 7) should be constrained by their phase contributions at the crossover frequency. The phase lag introduced by the current controller at ω_c should be:

$$\begin{aligned}\Delta\varphi_m &= \angle G_{\mathrm{pr+HC}}(z) \approx \angle G_{\mathrm{pr+HC}}(s) = \\ &\angle\Big(K\mathrm{p} + K\mathrm{r}\frac{2\xi\omega_0 s}{s^2 + 2\xi\omega_0 s + \omega_0^2} \\ &+ \sum_{h=5,7} K\mathrm{rh}\frac{2\xi_{\mathrm{h}} h\omega_0 s}{s^2 + 2\xi_{\mathrm{h}} h\omega_0 s + \omega_0^2}\Big)\end{aligned} \tag{12}$$

where $\Delta\varphi_m$ is the phase shifting at the crossover frequency introduced by the *PR+HC* regulator. For the proposed single-loop system, by setting φ_m=50°, $\Delta\varphi_{m1}$<5° and ΔI<3%, good dynamic and steady state performances can be ensured.

In Fig. 8, a Bode diagram of the designed closed-loop system is shown. The resonance peak on the AM-F curve is sufficiently suppressed, which means that the close-loop system does not amplify the harmonics around f_{res1}, which enhances the relative stability of the system. On the other hand, the AM-F and PH-F curves around f_0 are near 0dB and 0°, which leads to the superior tracking characteristic for the reference AC current. In addition, the PH-F curve at around $5f_0$ and $7f_0$ is obviously shifted close to 0° by the HC

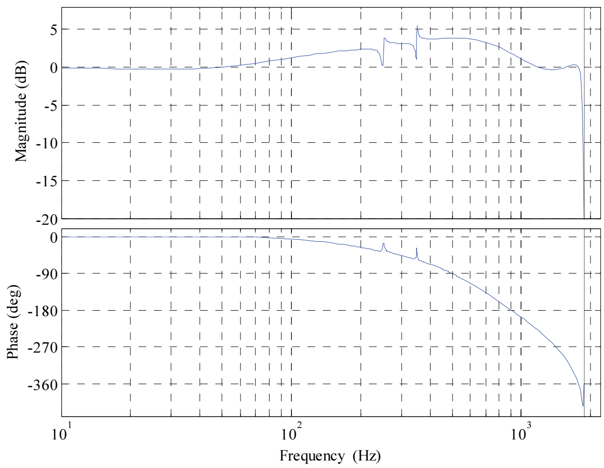

Fig. 8. Bode diagram of the proposed closed-loop system.

TABLE I
VSC SYSTEM PARAMETERS FOR EXPERIMENTS

Parameters	Value
System frequency f_0/Hz	50
Switching frequency f_s/Hz	3750
DC link voltage U_{dc}/V	290
Rated grid line to line voltage U_g/V	136
Rated output power P_{rate}/kW	11

controller, which mitigates the output harmonics at $5f_0$ and $7f_0$.

IV. EXPERIMENTAL VERIFICATION

To validate the superiority of the filtering performance of the proposed filter and the feasibility of the proposed control scheme, experiments are carried out in a scaled down 11kW three-phase PV grid-connected converter prototype. The parameters for the prototype are shown in Table I. A 2*Traps*+*RC* filter, the proposed improved multi-tuned filter, a conventional multi-tuned filter, and a *Trap*+*RC* filter are inserted between the converter and the utility grid to be the output filter. On the basis of complying with the regulations on harmonic currents in IEEE 1547, the compared filters are designed with the similar harmonic attenuation performance for the dominant high order switching harmonics. The designed parameters of the compared filters are listed in Table II. The design procedures are shown in Appendix B. Notice that the peak stored magnetic energy for the filtering branches of the different topologies are similar, while the grid side inductor of the 2*Traps*+*RC* filter and the improved multi-tuned filter are designed smaller thanks to their better harmonic attenuations. For the proposed improved multi-tuned filter, the proposed single-loop control scheme and the parameter design of the control system are adopted, with the T_{delay} selected as T_s. Meanwhile, the conventional PR controller is adopted for the compared topologies. The control circuit is equipped with a DSP chip TMS320F28335 at the core to implement, detect, and control, while the power device adopts three IGBT modules FF225R17ME4.

TABLE II
FILTER PARAMETERS FOR EXPERIMENTS

Parameters	*Trap*+*RC* filter	2*Traps*+*RC* filter	Conventional multi-tuned filter	Improved multi-tuned filter
L_i	270uH	270uH	270uH	270uH
L_g	350uH	220uH	350uH	200uH
C_1	50uF	40uF	50uF	50uF
C_2	—	20uF	20uF	20uF
L_1	36.1uH	45.1uH	36.1uH	36.1uH
L_2	—	22.5uH	22.5uH	22.5uH
R_1	0.09Ω	0.09Ω	0.35Ω	0.09Ω
R_2	—	0.09Ω	1Ω	0.09Ω
R_d	4Ω	20Ω	—	—
C_d	25uH	10uF	—	—

TABLE III
DOMINANT HIGH ORDER HARMONICS (%) FOR DIFFERENT FILTERS

Filters	Maximum harmonics around f_s	Maximum harmonics around $2f_s$	Maximum harmonics around $3f_s$ and above
Trap+*RC* filter	0.10%	0.41%	0.06%
2*Traps*+*RC* filter	0.16%	0.11%	0.09%
Conventional multi-tuned filter	0.23%	0.25%	0.05%
Improved multi-tuned filter	0.13%	0.09%	0.07%

TABLE IV
MEASURED POWER LOSS AND EFFICIENCY LOSS OF DIFFERENT PASSIVE FILTERS

Filters	Power Loss	Efficiency loss operating at full load
Trap+*RC* filter	43.4W	0.395%
2*Traps*+*RC* filter	32.7W	0.297%
Conventional multi-tuned filter	50.4W	0.458%
Improved multi-tuned filter	11.7W	0.106%

A. Filtering Performance Evaluation

To test the filtering performance, full load steady state experimental waveforms of the grid current I_g operating with the four different filters are illustrated in Fig. 9. Meanwhile, the corresponding dominant high order harmonics are listed in Table III.

It can be derived from Fig. 9 and Table III that the total harmonic current distortion (THD) of the experimental waveforms for the four filters are well below 3%, and that the

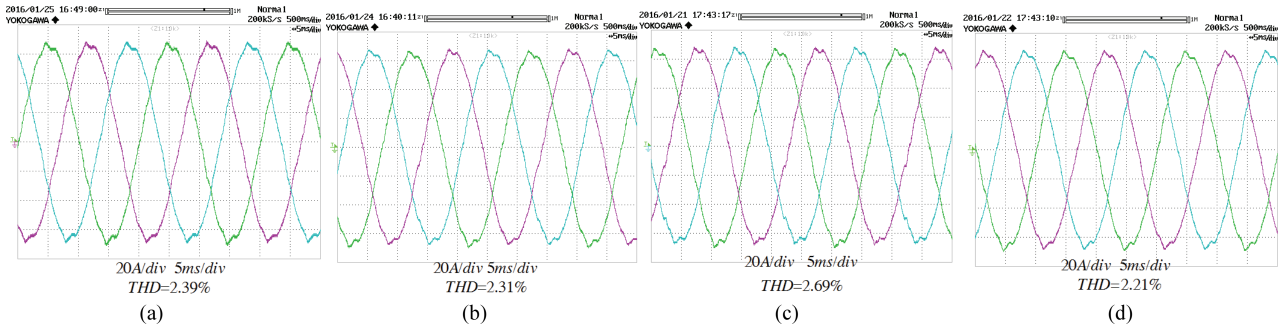

Fig. 9. Full load experimental waveforms obtained with four different filters (X-axis: time: 5*ms*/div; Y-axis: magnitude of the grid current: 20A/div): (a) *Trap*+RC filter; (b) 2*Traps*+RC filter; (c) conventional multi-tuned filer; (d) improved multi-tuned filter.

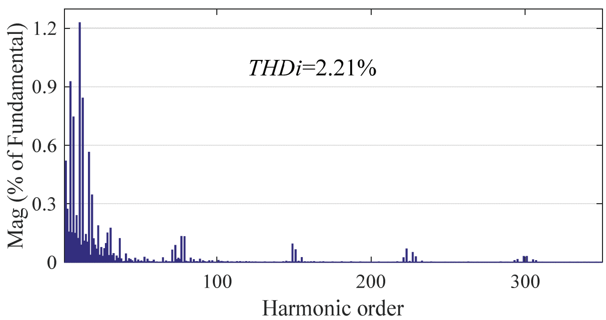

Fig. 10. Harmonic spectrum of I_g at a full load with the improved multi-tuned filter.

improved multi-tuned filter has the best high order harmonic attenuations among the compared filters, with the highest harmonics being around f_s, $2f_s$ and in the higher frequency band 0.13%, 0.09% and 0.07% under experimental circumstances.

B. Power Loss Measurement

Another major advantage of the proposed filter is its improved efficiency thanks to a reduction of the damping resistors in the branches. For the filters mentioned above, the power loss is measured by the experimental results. As listed in Table IV, the power loss of the improved multi-tuned filter is much less than that of other filters. Thus, it offers a great improvement in the efficiency of the whole PV VSC system.

C. Steady-State Performance Test

For the proposed improved multi-tuned filter, as shown in Fig. 9(a), the smooth steady-state waveform of the grid current I_g validates the effectiveness of the proposed control scheme. In Fig. 9(a), the RMS value of I_g is 46.83A, with an amplitude error of less than 2.5%, and the measured power factor is 0.995. The steady-state harmonic spectrum of I_g for the improved multi-tuned filter is shown in Fig.10. In Fig.10, the harmonics around f_{res1} (30th to 35th) are kept lower than 0.26%, which further verifies the effectiveness of the proposed control scheme in the elimination of the oscillations caused by the resonance peak. In addition, thanks to the *HC* controller, the 5th and 7th harmonic currents are reduced to 0.96% and 0.59%. The harmonic contents in the whole frequency band of I_g, shown in Fig.10, have complied with distortion limits specified by IEEE1547. All of the figures mentioned above show the good steady-state tracking feature and effective harmonic suppressions of the proposed control scheme.

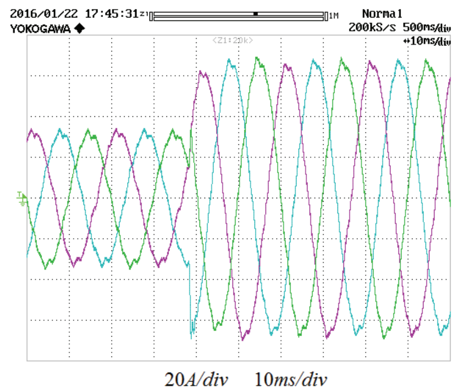

Fig. 11. Transient response of the grid side current I_g when the output current gets a step change from half load to full load.

D. Dynamic Performance Test

A dynamic waveform of the current when the output current has a step change from half load to full load is shown in Fig. 11. The quick step up and small overshoot of the current waveforms illustrate the good dynamic feature of the whole proposed system.

It can be derived from the experimental results above that the improved multi-tuned filter has better performance in terms of high order harmonic attenuation and power efficiency than the other high order filter topologies. On the other hand, no oscillations occur in the improved multi-tuned filter system and good steady-state and dynamic performances can be guaranteed, thanks to the proposed current control scheme.

V. Conclusions

In this paper, an improved design of a multi-tuned filter based on a digital control scheme for high power PV applications is proposed. The proposed filter topology can reduce the total inductance and power loss, while the proposed control scheme is simple and effective in terms of suppressing the resonance peak. Then, the following conclusions can be drawn.

1) The greatly reduced series resistor in the *LC* branches strengthens the harmonic attenuations at around f_s and $2f_s$, where high attenuations are required for PV VSC systems. When compared with common high order filters, the improved multi-tuned filter is able to sufficiently attenuate all of the major switching harmonics. Therefore, the total inductance is reduced to meet the regulatory requirements in IEEE1547.

2) The reduced damping resistor in the *LC* branches also decreases the operating power loss in the *LC* branches, which offers an increase in the efficiency of the PV system.

3) Thanks to the reduced total inductor, the resonance peak f_{res1} can be placed relatively high. Taking the digital delay into account, system stability and good control performance can be achieved by a grid current feedback single-loop controller with proper parameter determination.

Experimental results show the capability and application value of the proposed improved multi-tuned filter and the corresponding control strategy.

APPENDIX A

A schematic diagram of the proposed multi-tuned filter used in a grid-connected converter is illustrated in Fig. A-1.

Derived from Fig. A-1, a block diagram of the overall transfer function $G_{Ui\rightarrow Ig}(s)$ (shown in Equation 3) is constructed as shown in Fig.A-2.

In Fig. A-2, $Z_{\text{branch}}(s)$ is the equivalent impedance of the two paralleled *RLC* branches. The specific expression of $Z_{\text{branch}}(s)$ is:

$$\begin{cases} Z_{\text{branch}}(s) = Z_1 // Z_2 = \dfrac{Z_1 Z_2}{Z_1 + Z_2} \\ Z_1 = L_1 s + R_1 + \dfrac{1}{C_1 s} \\ Z_2 = L_2 s + R_2 + \dfrac{1}{C_2 s} \end{cases} \tag{13}$$

Assuming that the grid is an ideal voltage source, the transfer function $G_{Ui\rightarrow Ig}(s)$ can be derived from Fig. A-2.

$$\begin{aligned} G_{U\text{i}\rightarrow I\text{g}}(s) &= \frac{I_\text{g}(s)}{U_\text{i}(s)} \bigg|_{U_\text{g}=0} \\ &= \frac{Z_{\text{branch}}(s)}{L_\text{g} L_\text{i} s^2 + (L_\text{g} + L_\text{i}) s \cdot Z_{\text{branch}}(s)} \end{aligned} \tag{14}$$

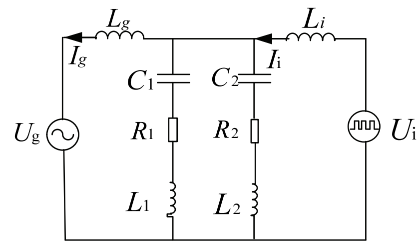

Fig. A-1. Schematic diagram of the multi-tuned filter used in a grid-connected converter.

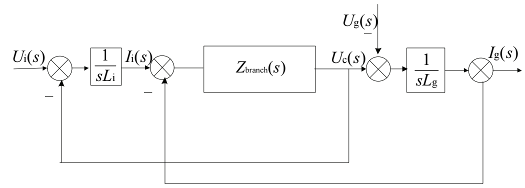

Fig. A-2. Block diagram of the overall transfer function $G_{Ui\rightarrow Ig}(s)$.

By combining (13) and (14), the transfer function $G_{Ui\rightarrow Ig}(s)$ is deduced as:

$$G_{U\text{i}\rightarrow I\text{g}}(s) = \frac{as^4 + bs^3 + cs^2 + ds + e}{fs^5 + gs^4 + hs^3 + is^2 + js} \tag{15}$$

where $a = C_1C_2L_1L_2$,
$b = C_1C_2L_1R_2 + C_1C_2L_2R_1$,
$c = C_1L_1 + C_2L_2 + C_1C_2R_1R_2$,
$d = C_1R_1 + C_2R_2$,
$e = 1$,
$f = C_1C_2L_1L_2\,(L_g + L_i) + C_1C_2L_gL_i(L_1 + L_2)$,
$g = C_1C_2R_2(L_1L_g + L_1L_i + L_gL_i) + C_1C_2R_1(L_2L_g + L_2L_i + L_gL_i)$,
$h = C_1L_1(L_g + L_i) + C_2L_2(L_g + L_i) + L_gL_i(C_1 + C_2)$
$\quad + C_1C_2R_1R_2(L_g + L_i)$,
$i = C_1L_gR_1 + C_2L_gR_2 + C_1L_iR_1 + C_2L_iR_2$,
$j = L_g + L_i$
where (15) is the same as equation (3).

APPENDIX B

The step-by-step design procedure of the proposed multi-tuned filter has been applied to the experimental setup (shown in Table I) as a design example. Step 1 and step 2 of the procedure are similar to the design procedure shown in [8], and the specific procedure is as follows:

1) Adopting a 60% current ripple for the converter-side inductor L_i, L_i is calculated to be more than 244μH, and it is selected as 270μH.

2) To ensure that the total reactive power loss in the *LC* trap branches is less than 5% of the rated power, the sum of the capacitor value in each of the branches is designed to be $C_1 + C_2 \leq 94.7\mu F$. Then, $C_1 + C_2 = 70\mu F$ is selected so that the reactive power of the capacitor is limited to 3.7% of the rated power.

3) By placing the resonance frequency of the *LC* traps at f_s and $2f_s$, the parameters in the *LC* branches are restrained as follows:

$$f_s = \frac{1}{2\pi}\sqrt{\frac{1}{L_1C_1}} \tag{16}$$

$$2f_s = \frac{1}{2\pi}\sqrt{\frac{1}{L_2C_2}} \tag{17}$$

When designing the parameter values in the *LC* trap branches, since C_1+C_2=70μF, by combining (2), (16) and (17) simultaneously, the capacitor values of C_1 and C_2 can be theoretically calculated at 51.85μF and 18.15μF. Then, C_1=50μF and C_2=20μF are suitable for actual choices. The corresponding inductor values of L_1 and L_2 are calculated as 36.1μH and 22.5μH.

4) By setting the Q factors of the two *LC* branches as 10, as discussed in Section II, the equivalent resistor values R_1 and R_2 can be calculated as 0.085Ω and 0.106 Ω. Then, R_1 and R_2 are both designed as 0.09Ω.

5) The grid-side inductor L_g is limited to between 135.9μH and 770.7μH according to (1). On the other hand, the maximum value of L_g+L_i should be less than 0.1pu (923μH) [2], which means that L_g should be less than 653μH. By considering a large enough margin for the series equivalent inductance of the utility grid, L_g is then chosen as 200μH.

The design procedures for the other high order tuned-type filters: *Trap+RC* filter, conventional multi-tuned filter and 2*Traps+RC* filter are shown in [5], [6] and [8], respectively.

ACKNOWLEDGMENT

This work was supported by Program of the National Natural Science Foundation of China under Grant 51577128, and Key Project of Smart Grid Technology and Equipment of National Key Research and Development Plan of China (2016YFB0900600).

REFERENCES

[1] R. Teodorescu, M. Liserre, and R. Rodriguez, *Grid Converters for Photovoltaic and Wind Power Systems*, Wiley, John Wiley & Sons, 2011.

[2] Z. Zou, Z. Wang, and M. Cheng, "Modeling, analysis, and design of multifunction grid-interfaced inverters with output *LCL* filter," *IEEE Trans. Power Electron*. Vol. 29, No. 7, pp. 3830−3839, Jul. 2014.

[3] F. Liu, X. Zha, and S. Duan, "Design and research of *LCL* filter of three phase grid-connected inverter," *Journal of Electrician Technology*, Vol. 25, No. 3, pp. 110-116, 2010.

[4] A. A. Rockhill, M. Liserre, R. Teodorescu, and P. Rodriguez, "Grid-filter design for a multi-megawatt voltage-source inverter," *IEEE Trans. Ind. Electron.,* Vol. 58, No. 4, pp. 1205-1217, Apr. 2011.

[5] S. Piasecki, "High order line filters for grid connected AC-DC converter-parameters selection and optimization," in *23rd IEEE International Symposium on Industrial Electronics (ISIE)*, pp. 2687-2692, Jun. 2014.

[6] J. M. Bloemink and T. C. Green. "Reducing passive filter sizes with tuned traps for distribution level power electronics," in *Proceedings of the 14th European Conference on Power Electronics and Applications (EPE)*, Aug./Sep. 2011.

[7] J. F. Moynihan, M. G. Egan, and J. M. D. Murphy, "Theoretical spectra of space-vector-modulated waveforms," *IEEE Proceedings of Electric Power Applications*, Vol. 145, No. 1, pp. 17-24, Jan. 1998.

[8] J. Xu, J. Yang, J. Ye, Z. Zhang, and A. Shen, "An *LTCL* filter for three-phase grid-connected converters," *IEEE Trans. Power Electron.*, Vol. 29, No. 8, pp. 4322-4338, Aug. 2014.

[9] R. N. Beres, X. Wang, M. Liserre, F. Blaabjerg, and C. L. Bak,, "A review of passive power filters for three-phase grid-connected voltage-source converters," *IEEE Journals of Emerging and Selected Topics in Power Electronics*, Vol. 4, No. 1, pp. 54-69, Mar. 2016.

[10] R. N. Beres, X. Wang, F. Blaabjerg, M. Liserre, and C. L. Bak, "Optimal design of high-order passive-damped filters for grid-connected applications," *IEEE Trans. Power Electron.*, Vol. 31, No. 3, pp. 2083-2098, Mar. 2016.

[11] W. Wu, Y. He, and F. Blaabjerg, "An *LLCL*-power filter for single-phase grid-tied inverter," *IEEE Trans. Power Electron.*, Vol. 27, No. 2, pp. 782-789, Feb. 2012.

[12] W. Wu, Y. Sun, M. Huang, X. Wang, H. Wang, F. Blaabjerg, M. Liserre, and H. S. H. Chung, "A robust passive damping method for *LLCL*-filter-based grid-tied inverters to minimize the effect of grid harmonic voltages," *IEEE Trans. Power Electron.*, Vol. 29, No. 7, pp. 3279-3289, Jul. 2014.

[13] X. Zhang, J. W. Spencer, and J. M. Guerrero, "Small-signal modeling of digitally controlled grid-connected inverters with LCL filters," *IEEE Trans. Ind. Electron.*, Vol. 60, No. 9, pp. 3752-3765, Sep. 2013.

[14] J. Yin, S. Duan, and B. Liu, "Stability analysis of grid-connected inverter with LCL filter adopting a digital single-loop controller with inherent damping characteristic," *IEEE Trans. Ind. Informat.*, Vol. 9, No. 2, pp. 1104-1112, May 2013.

[15] A. M. Cantarellas, E. Rakhshani, D. Remon, and P. Rodriguez. "Design of the LCL+trap filter for the two-level VSC installed in a large-scale wave power plant," in *IEEE Energy Conversion Congress and Exposition (ECCE)*, pp. 707−712, Sep. 2013.

[16] W. Wu, Y. He, T. Tang, and F. Blaabjerg, "A new design method for the passive damped LCL and LLCL-filter based single-phase grid-tied inverter," *IEEE Trans. Ind. Electron*., Vol. 60, No. 10, pp. 4339-4350, Oct. 2013.

[17] J. K. Phipps, "A transfer function approach to harmonic filter design," *IEEE Ind. Appl. Mag.*, Vol. 3, No. 2, pp. 68-82, Mar./Apr. 1997.

[18] R. Peña-Alzola, M. Liserre, F. Blaabjerg, R. Sebastián, J. Dannehl, and F. W. Fuchs, "Analysis of the passive damping losses in LCL-filter based grid converters," *IEEE Trans. Power Electron*., Vol. 28, No. 6, pp. 2642-2646, Jun. 2013.

[19] M. Orellana and R. Grino, "On the stability of discrete-time active damping methods for VSI converters with a *LCL* input filter," in *38th Annual Conference on IEEE Industrial Electronics Society (IECON)*, Oct. 2012.
[20] R. Peña-Alzola, M. Liserre, F. Blaabjerg, R. Sebastián, J. Dannehl, and F. W. Fuchs, "Systematic design of the lead-lag network method for active damping in LCL-filter based three phase converters," *IEEE Trans. Ind. Informat.*, Vol. 10, No. 1, pp. 43-52, Feb. 2014.
[21] M. Hanif, V. Khadkikar, W. Xiao, and J. L. Kirtley, "Two degrees of freedom active damping technique for *LCL* filter-based grid connected PV systems," *IEEE Trans. Ind. Electron.*, Vol. 61, No. 6, pp. 2795-2803, Jun. 2014.
[22] S. G. Parker, B. P. McGrath, and D. G. Holmes, "Regions of active damping control for *LCL* filters," *IEEE Trans. Ind. Appl.*, Vol. 50, No. 1, pp. 424-432, Jan./Feb. 2014.
[23] C. Zou, B. Liu, S. Duan, and R. Li, "Influence of delay on system stability and delay optimization of grid-connected inverters with *LCL* filter," *IEEE Trans. Ind. Informat.*, Vol. 10, No. 3, pp. 1775-1783, Aug. 2014.
[24] H. Shan, Y, Kang, X. Kong, Z. Liu, M. Yu, H. Li, F. Luo, and L. Liu, "The research on the digital controlled effect of performance on the PWM inverter," in *IEEE 30th International Telecommunications Energy Conference (INTELEC)*, Sep. 2008.
[25] S. Buso and P. Mattavelli, *Digital Control in Power Electronics*, Morgan and Claypool, 2006.
[26] J. Dannehl, C. Wessels, and F. W. Fuchs, "Limitations of voltage-oriented PI current control of grid-connected PWM rectifiers with *LCL* filters," *IEEE Trans. Ind. Electron.*, Vol. 56, No. 2, pp. 380-388, Feb. 2009.
[27] D. G. Holmes, T. A. Lipo, B. P. McGrath, and W. Y. Kong, "Optimized design of stationary frame three phase AC current regulators," *IEEE Trans. Power Electron*., Vol. 24, No. 11, pp.2417-2425, Nov. 2009.
[28] C. Bao, X. Ruan, X. Wang, W. Li, D. Pan, and K. Weng, "Step-by-step controller design for *LCL*-type grid-connected inverter with capacitor-current-feedback active-damping," *IEEE Trans. Power Electron.*, Vol. 29, No. 3, pp. 1239-1253, Mar. 2014.

Guangyu Sun was born in Liaoning, China, in 1990. He received his B.S. degree in Electrical Engineering from Tianjin University, Tianjin, China, in 2012; where he is presently working towards his Ph.D. degree in the Department of Electrical Engineering and Automation. His current research interests include the design of grid interface filters for converters, the control of power engineering applications, and the power quality control of microgrids and distribution networks.

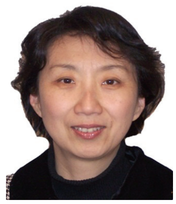

Yongli Li was born in Hebei, China, in 1963. She received her B.S. and M.S. degrees in Electrical Engineering from Tianjin University, Tianjin, China, in 1984 and 1987, respectively; and her Ph.D. degree in Electrical Engineering from the Universite Libre de Bruxelles, Brussels, Belgium, in 1993. She is presently working as a Professor in the Department of Electrical Engineering and Automation, Tianjin University. Her current research interests include the fault analysis of power systems, the fault diagnosis of electrical equipment, the protection and adaptive reclosing of EHV/UHV transmission systems, and the protection and control of microgrids and distribution networks.

Wei Jin was born in Shanxi, China, in 1990. He received his B.S. degree in Electrical Engineering from Tianjin University, Tianjin, China, in 2013, where he is presently working towards his Ph.D. degree in the Department of Electrical Engineering and Automation. His current research interests include control technology for converters, and power quality control of microgrids and distribution networks.